Available online at www.sciencedirect.com
ScienceDirect
International Journal of Thermal Sciences 45 (2006) 1091–1102
International Journal of Thermal Sciences
www.elsevier.com/locate/ijts

Compact models for transient conduction or viscous transport in non-circular geometries with a uniform source ☆

Y.S. Muzychka [a,*], M.M. Yovanovich [b]

[a] *Faculty of Engineering and Applied Science, Memorial University of Newfoundland, St. John's, NL, Canada A1B 3X5*
[b] *Department of Mechanical Engineering, University of Waterloo, Waterloo, ON, Canada N2L 3G1*

Received 10 September 2005; accepted 1 February 2006

Available online 2 March 2006

Abstract

Transient heat conduction in solid prismatic bars of constant cross-sectional area having uniform heat generation and unsteady momentum transport in infinitely long ducts of arbitrary but constant cross-sectional area are examined. In both cases the solutions are mathematically modeled using a transient Poisson equation. By means of scaling analysis a general asymptotic model is developed for an arbitrary non-circular cross-section. Further, by means of a novel characteristic length scale, the solutions for a number of fundamental shapes are shown to be weak functions of geometry. The proposed models can be used to predict the dimensionless mean flux at the wall and the area averaged temperature or velocity for the tube, annulus, channel and rectangle for which exact series solutions exist. Due to the asymptotic nature of the proposed models, it is shown that they are also applicable to other shapes at short and long times for which no solutions or data exist. The root mean square (RMS) error based on comparisons with exact results is between 2.2–7.6 percent for all data considered.

Keywords: Unsteady viscous flow; Unsteady heat conduction; Modelling; Asymptotic analysis; Scale analysis; Poisson equation

1. Introduction

This paper is concerned with the analysis of unsteady transport of momentum due to a suddenly imposed constant pressure gradient or unsteady heat conduction due to a uniformly distributed heat source in circular and non-circular geometries.

The viscous transport problem which is most often found in advanced level fluids texts [1–5], is concerned with start up flow in circular and non-circular tubes and channels. The solution for a tube was originally found by Szymanski [6] in 1932. In addition to the circular tube, solutions for the parallel plate channel [7,8], circular annulus [9], and rectangle [10], are also available in the fluids literature. The solution for the channel is discussed in Rouse [7] and Arpaci and Larsen [8] with no reference to its origins. The solution may be traced back to Lamb [11] as early as 1927. Lamb [11] used a Fourier series method to obtain the solution, but later Bromwich [12] obtained a similar solution using Laplace transforms [12,13]. The solution for the circular annulus was obtained by Müller [9] in 1936. While the solution for a rectangular channel may be found in Erdogan [10], but elements of its solution are discussed in earlier mathematical works [14–17]. The solution for the rectangle as presented by Erdogan [10] is somewhat complex and has been re-solved using Fourier transforms [18–20] as part of the present work to provide a more compact form.

The viscous transport problem also has an analogous counterpart in conduction heat transfer. The temperature field which results from a uniformly distributed heat source which is suddenly turned on is governed by a similar differential equation and boundary and initial conditions [21]. Carslaw and Jaeger [21] discuss both the plane wall and circular cylinder solutions for transient conduction with a constant uniform heat source. A solution for the annular cylinder is not presented, but cited by Thews [22]. No reference to any solution for a rectangular domain is made.

The paper reviews the aforementioned analytical solutions and considers the characteristics of these solutions. Simple

☆ A preliminary version of this paper was presented at IMECE-04 International Mechanical Engineering Congress and Exposition, November 13–19, 2004, Anaheim, CA.

* Corresponding author.
E-mail address: yuri@engr.mun.ca (Y.S. Muzychka).

1290-0729/$ – see front matter
doi:10.1016/j.ijthermalsci.2006.02.002

Nomenclature

A	area	m^2
A_0, A_∞	closure constants	
B_0, B_∞		
a, b	major and minor axes of rectangle	m
	outer and inner radii	m
D_h	hydraulic diameter, $\equiv 4A/P$	
$f\,Re_{\mathcal{L}}$	friction factor Reynolds number group $\equiv 2Po_{\mathcal{L}}$	
$\mathcal{G}$	source parameter	
$J_0(\cdot)$	Bessel function of first kind order zero	
k	thermal conductivity	$W\,m^{-1}K^{-1}$
L	duct or channel length	m
$\mathcal{L}$	arbitrary length scale	m
m, n	series indices	
n, p	asymptotic correlation parameters	
n	directed normal	m
N	number of sides of a polygon	
p	pressure	Pa
P	perimeter	m
$Po_{\mathcal{L}}$	Poiseuille number, $\equiv \tau\mathcal{L}/\mu\overline{w}$	
q_s	surface heat flux	$W\,m^{-2}$
r	radial coordinate	m
r^*	radii ratio, b/a	
$Re_{\mathcal{L}}$	Reynolds number, $\equiv \overline{w}\mathcal{L}/\nu$	
s	arc length	m
$\mathcal{S}$	volumetric heat generation	$W\,m^{-3}$
t	time	s
$t^\star$	dimensionless time, $\equiv \beta t/\mathcal{L}^2$	
w	velocity	$m\,s^{-1}$
$\overline{w}$	average velocity	$m\,s^{-1}$
x, y, z	Cartesian coordinates	m
$Y_0(\cdot)$	Bessel function of second kind order zero	

Greek symbols

α	thermal diffusion coefficient	$m^2\,s^{-1}$
β	general diffusion coefficient	$m^2\,s^{-1}$
δ	boundary layer thickness	m
δ_n	eigenvalue	
ε	aspect ratio, b/a	
ϕ	independent variable, θ or w	
$\phi^\star$	dimensionless transport quantity, $\equiv \overline{\phi}/\mathcal{G}\mathcal{L}^2$	
ϕ_n	gradient of ϕ, $\equiv \partial\phi/\partial n$	
γ	transport coefficient, k or μ	
η	similarity variable	
λ_{mn}	eigenvalue	
μ	dynamic viscosity	$Ns\,m^{-2}$
ν	kinematic viscosity	$m^2\,s^{-1}$
θ	temperature excess	K
ρ	density	$kg\,m^{-3}$
ϱ	dimensionless radial position, r/a	
ψ	flux	$W\,m^{-2}$ or $N\,m^{-2}$
$\phi^\star$	dimensionless flux, $\equiv \overline{\phi}_n P/A\mathcal{G}$	
τ_w	wall shear stress	Pa

Subscripts

s	surface
w	wall
∞	steady state value
$\mathcal{L}$	based upon the arbitrary length $\mathcal{L}$

Superscripts

$\overline{(\cdot)}$	mean value
$(\cdot)^\star$	dimensionless value

models are proposed for calculating these characteristics which make computations more amenable. Two advantages of these compact models will become apparent. First, the available solutions are in the form of infinite series. In the case of the rectangle a double infinite series is required. Further, the solutions for the cylinder and annulus involve Bessel functions and the eigenvalues must be numerically computed from expressions involving these functions. Second, the analysis will show that the results are applicable to other useful geometries for which no solutions exist, i.e. the elliptic duct, triangular duct, and polygonal ducts (refer to Fig. 1). With respect to the problem of interest, two fundamental quantities are useful to the engineer for modeling the transient response of a system. One is the dimensionless area averaged velocity or temperature (potential), and the other is the dimensionless perimeter averaged wall shear or heat flux (gradient of potential). Since the solutions to these problems involve infinite single and double series, it is desirable to have compact models for computing the desired parameters. Simple models will be proposed for both the dimensionless average potential and dimensionless average gradient of the potential.

In general, the results presented in this work are applicable to any unsteady Poisson equation with constant uniformly distributed source, constant physical properties, and homogeneous Dirichlet boundary conditions. Next the mathematical statement for each problem is discussed and presented in a general form.

2. Problem statement

The problem of interest is characterized by the following general Poisson equation:

$$\frac{1}{\beta}\frac{\partial\phi}{\partial t} = \mathcal{G} + \nabla^2\phi \tag{1}$$

which is subject to the boundedness condition along the axis of the geometry, $\phi \neq \infty$, homogeneous Dirichlet conditions at the boundary, $\phi = 0$, and the initial condition $\phi = 0$, when $t = 0$. The system is shown in Fig. 2. It consists of an infinitely long duct or cylinder of arbitrary but constant cross-sectional area, A, bounded by perimeter, P.

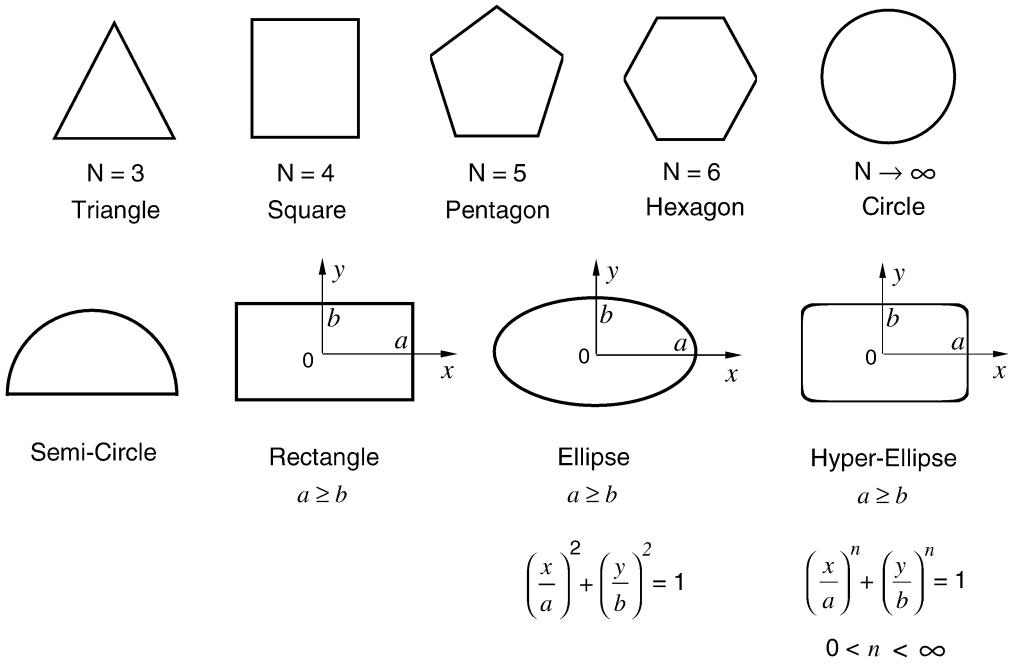

Fig. 1. Typical non-circular cross-sections.

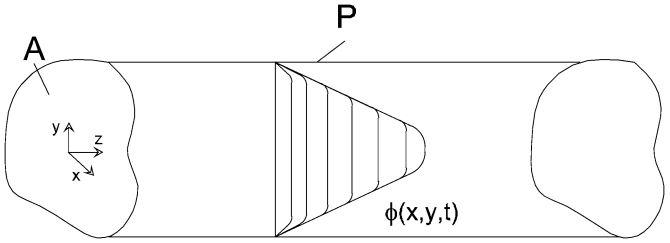

Fig. 2. System under consideration.

Table 1
Summary of variables

Problem	ϕ	β	$\mathcal{G}$	γ	ψ
Momentum	w	ν	$\frac{1}{\mu}\frac{\Delta p}{L}$	μ	$\tau_w=\mu\frac{\partial w}{\partial n}$
Conduction	θ	α	$\frac{\mathcal{S}}{k}$	k	$q_s=k\frac{\partial\theta}{\partial n}$

It is of interest to obtain the area mean potential, obtained by integrating the solution for ϕ over the cross-sectional area:

$$\overline{\phi}(t)=\frac{1}{A}\iint_A \phi\,\mathrm{d}A \tag{2}$$

Also, of interest is the perimeter averaged or mean gradient at the surface, $\overline{\frac{\partial\phi}{\partial n}}\equiv\overline{\phi}_n$:

$$\overline{\psi}(t)=\frac{1}{P}\oint \gamma\frac{\partial\phi}{\partial n}\,\mathrm{d}s=\gamma\overline{\phi}_n \tag{3}$$

which is related to the momentum flux or heat flux through the appropriate thermophysical property for γ using Newton's law or Fourier's law. The two fundamental transport problems are summarized below in Table 1.

2.1. Unsteady viscous transport

The momentum transport or impulsively started flow problem is often classified in some texts as Rayleigh flow, Telionis [4]. In other texts it is referred to as startup flow or the commencement of Poiseuille flow. In this problem, the source is defined as $\mathcal{G}=\frac{1}{\mu}\frac{\Delta p}{L}$. The dimensionless mean velocity is:

$$w^\star=\frac{\overline{w}}{\mathcal{L}^2\frac{1}{\mu}\frac{\Delta p}{L}}=\frac{\overline{\phi}}{\mathcal{G}\mathcal{L}^2}=\phi^\star \tag{4}$$

While the dimensionless momentum flux (or shear stress) at the surface is defined with respect to the steady state value:

$$\tau^\star=\frac{\tau_w}{\tau_\infty} \tag{5}$$

where

$$\tau_\infty=\frac{A}{P}\frac{\Delta p}{L} \tag{6}$$

is obtained from the steady state force balance.

This leads to the following result for the dimensionless momentum flux or wall shear:

$$\tau^\star=\frac{\tau_w}{\frac{A}{P}\frac{\Delta p}{L}}=\frac{\mu\overline{\phi}_n}{\frac{A}{P}\frac{\Delta p}{L}}=\frac{\overline{\phi}_n}{\frac{A}{P}\mathcal{G}}=\psi^\star \tag{7}$$

2.2. Unsteady heat conduction

In the case of unsteady heat conduction with a source, similar dimensionless groups may be defined. In this problem, the source is defined as $\mathcal{G}=\mathcal{S}/k$. The dimensionless mean temperature in the cross-section is:

$$\theta^\star=\frac{\overline{\theta}}{\mathcal{L}^2\frac{\mathcal{S}}{k}}=\frac{\overline{\phi}}{\mathcal{G}\mathcal{L}^2}=\phi^\star \tag{8}$$

While the dimensionless heat flux at the surface is defined with respect to the steady state value:

$$q^\star = \frac{q_s}{q_\infty} \tag{9}$$

where

$$q_\infty = \frac{A}{P}\mathcal{S} \tag{10}$$

is obtained from the steady state heat balance.

This leads to the following result for the dimensionless heat flux:

$$q^\star = \frac{q_s}{\frac{A}{P}\mathcal{S}} = \frac{k\overline{\phi}_n}{\frac{A}{P}\mathcal{S}} = \frac{\overline{\phi}_n}{\frac{A}{P}\mathcal{G}} = \psi^\star \tag{11}$$

In later sections, we will examine exact results and approximate results for the two dimensionless quantities, $\phi^\star$ and $\psi^\star$. In the next section, we use scale analysis to obtain the order of magnitude behaviour for both quantities in terms of asymptotic limits.

3. Scale analysis

In this section, we will examine what information the method of scale analysis [23] may provide. Recall, the transport equation:

$$\underbrace{\frac{1}{\beta}\frac{\partial\phi}{\partial t}}_{\text{Storage}} = \underbrace{\mathcal{G}}_{\text{Generation}} + \underbrace{\nabla^2\phi}_{\text{Diffusion}} \tag{12}$$

This equation represents a balance of three quantities: storage, generation, and diffusion. There are three distinct flow regions in this problem that may be considered. Fully developed flow exists after a very long time, and at short times, there exists a potential core and a very thin boundary layer region. Each of these regions may be analyzed using scale analysis. The following scales will be used: $\phi \sim \overline{\phi}$, $t \sim t$, and $\nabla^2 \sim 1/\mathcal{L}^2$ for long time and $\nabla^2 \sim 1/\delta^2$ for short time. Here, $\mathcal{L}$ is as yet undetermined characteristic length scale related to the geometry and δ is the boundary layer thickness or penetration scale associated with early times.

First for long times $t \to \infty$, or fully developed flow, the balance between generation and diffusion leads to $\nabla^2 \sim 1/\mathcal{L}^2$. This gives

$$\frac{\overline{\phi}}{\mathcal{L}^2} \sim \mathcal{G} \tag{13}$$

or

$$\overline{\phi} \sim \mathcal{G}\mathcal{L}^2 \tag{14}$$

or

$$\phi^\star_\infty = \frac{\overline{\phi}}{\mathcal{G}\mathcal{L}^2} \sim 1 \quad \text{as } t \to \infty \tag{15}$$

Next, for short times $t \to 0$, the balance is between storage and generation, or considering the potential core, this leads to

$$\frac{1}{\beta}\frac{\overline{\phi}}{t} \sim \mathcal{G} \tag{16}$$

or

$$\overline{\phi} \sim \mathcal{G}\beta t \tag{17}$$

or

$$\phi^\star_0 \sim \frac{\beta t}{\mathcal{L}^2} \sim t^\star \quad \text{as } t \to 0 \tag{18}$$

Next, in the boundary layer region, the balance between storage and diffusion leads to $\nabla^2 \sim 1/\delta^2$. This gives

$$\frac{1}{\beta}\frac{\overline{\phi}}{t} \sim \frac{\overline{\phi}}{\delta^2} \tag{19}$$

or

$$\delta \sim \sqrt{\beta t} \tag{20}$$

which is the intrinsic penetration depth.

The flow becomes fully developed when $\delta \sim \mathcal{L}$, such that

$$\beta t \sim \mathcal{L}^2 \tag{21}$$

or

$$t^\star \sim \frac{\beta t}{\mathcal{L}^2} \sim 1 \tag{22}$$

Finally, we wish to develop expressions for the mean flux at the surface defined as:

$$\overline{\psi} = \gamma\overline{\frac{\partial\phi}{\partial n}} \tag{23}$$

We must consider the two limiting cases of short time and long time. For long time, $t \to \infty$, the flux becomes:

$$\overline{\psi} \sim \gamma\frac{\overline{\phi}}{\mathcal{L}} \tag{24}$$

We may also relate the flux to the source $\mathcal{G}$ for fully developed flows, where

$$\overline{\psi}_\infty = \frac{A}{P}\mathcal{G}\gamma \tag{25}$$

Thus, if we define $\psi^\star = \psi/\psi_\infty$, we obtain

$$\psi^\star_\infty = \frac{\overline{\phi}}{(\frac{A}{P}\mathcal{G}\mathcal{L})} \sim 1 \quad \text{as } t \to \infty \tag{26}$$

Finally, for short times, $t \to 0$, the flux becomes

$$\overline{\psi} \sim \frac{\gamma\overline{\phi}}{\delta} \tag{27}$$

Also, from the transport equation we see that

$$\frac{\overline{\phi}}{\delta^2} \sim \mathcal{G} \tag{28}$$

or, after combining Eqs. (27) and (28):

$$\overline{\psi} \sim \gamma\mathcal{G}\delta \tag{29}$$

Finally defining $\psi^\star$ as before, we obtain

$$\psi^\star_0 \sim \frac{\delta}{A/P} \sim \frac{\sqrt{t^\star}\mathcal{L}}{A/P} \quad \text{as } t \to 0 \tag{30}$$

It is clear from scaling analysis, that two distinct characteristics are present. These are the dimensionless mean potential,

$\phi^\star$ and dimensionless mean surface flux, $\psi^\star$. Each has the following asymptotic behaviour:

$$\phi^\star = \begin{cases} A_0 t^\star & t^\star \to 0 \\ A_\infty & t^\star \to \infty \end{cases} \tag{31}$$

and

$$\psi^\star = \begin{cases} B_0 \sqrt{t^\star} & t^\star \to 0 \\ B_\infty & t^\star \to \infty \end{cases} \tag{32}$$

Later, an approximate model is obtained by superposing these asymptotes. But first we examine the exact solutions for each of these regions in order to determine the closure constants A_0, A_∞, B_0, and B_∞.

4. Asymptotic behaviour

The exact asymptotic behaviour for small and large times may now be examined for each dimensionless quantity of interest.

4.1. Long time—$t \to \infty$

For long time, $t \to \infty$, the flow is characterized by a balance between generation and diffusion. This problem has been analyzed extensively for momentum transport and solutions to some forty configurations may be found in Shah and London [24]. The results are usually presented in the form of the dimensionless group $f\,Re$, the *Fanning* friction factor Reynolds number product defined as:

$$\frac{f\,Re_{\mathcal{L}}}{2} = \frac{\overline{\tau}_\infty \mathcal{L}}{\mu \overline{w}} = \frac{\overline{\psi}_\infty \mathcal{L}}{\gamma \overline{\phi}} = Po_{\mathcal{L}} \tag{33}$$

where Po is referred to in the fluids literature as the Poiseuille number [4].

We can further introduce the source term through the fully developed flow balance Eq. (25) and obtain:

$$Po_{\mathcal{L}} = \frac{\overline{\psi}_\infty \mathcal{L}}{\gamma \overline{\phi}} = \frac{\frac{A}{P}\mathcal{G}\mathcal{L}}{\overline{\phi}} \tag{34}$$

Rearranging, for $\overline{\phi}$ and using the definition of the dimensionless mean potential, Eq. (4) or Eq. (8), we obtain

$$\phi^\star = \frac{A/P}{Po_{\mathcal{L}}\mathcal{L}} \tag{35}$$

which gives

$$A_\infty = \frac{A/P}{Po_{\mathcal{L}}\mathcal{L}} \tag{36}$$

Finally, by virtue of the definition of the dimensionless flux, Eq. (5) or Eq. (9) and the value for ψ_∞, the dimensionless asymptotic limit for $\psi^\star$ is:

$$\psi^\star = 1 \tag{37}$$

which gives

$$B_\infty = 1 \tag{38}$$

4.2. Short time—$t \to 0$

For short times, $t \to 0$, the transport is characterized by a balance between generation and storage. The equation of transport which may be solved in the potential core when δ is small is:

$$\frac{1}{\beta}\frac{\partial \phi}{\partial t} = \mathcal{G} \tag{39}$$

This may be integrated and solved with the initial condition $\phi(0) = 0$ to give:

$$\phi(t) = \beta t \mathcal{G} \approx \overline{\phi}(t) \tag{40}$$

When non-dimensionalized, the solution for short time in the potential core is:

$$\phi^\star = \frac{\beta t}{\mathcal{L}^2} = t^\star \tag{41}$$

which gives

$$A_0 = 1 \tag{42}$$

The short time flux may be found by considering the classic Stokes solution for momentum transport or heat conduction into a half space. The solution for the field resulting from a step change at the surface is:

$$\phi = \phi_o \operatorname{erfc}(\eta) \tag{43}$$

where $\eta = x/2\sqrt{\beta t}$.

The result for the boundary layer thickness which accounts for the mean penetration of the field from the surface to the potential core, i.e. the area under the curve defined by Eq. (43), may be written as [25]:

$$\delta\phi_o = 2\sqrt{\beta t}\int_0^\infty \phi_o \operatorname{erfc}(\eta)\,\mathrm{d}\eta \tag{44}$$

which gives

$$\delta = \frac{2}{\sqrt{\pi}}\sqrt{\beta t} \approx 1.128\sqrt{\beta t} \tag{45}$$

Eq. (45) accounts for the mean depth of penetration of the field to the potential region. Although the potential core is in a state of change, the process is still applicable, since we are interested in the characteristics of the boundary layer which is bounded by the surface and the potential core. In the case of momentum transport, this boundary layer defines the total mass flow, $U\delta$, at any time which results from the impulsive motion of an infinite flat plate. In the case of heat conduction, the boundary layer defines the total energy stored in the field, $\theta_o \delta \rho C_p A$, at any time after the step change has occurred. This is shown graphically in Fig. 3. It may be viewed as the accumulated mean boundary layer thickness. Similar results may also be obtained by integrating the boundary flux between $t = 0$ and an arbitrary time $t = t$.

Using this result in Eq. (30) gives:

$$\psi^\star = \frac{2}{\sqrt{\pi}}\frac{P\mathcal{L}}{A}\sqrt{t^\star} \tag{46}$$

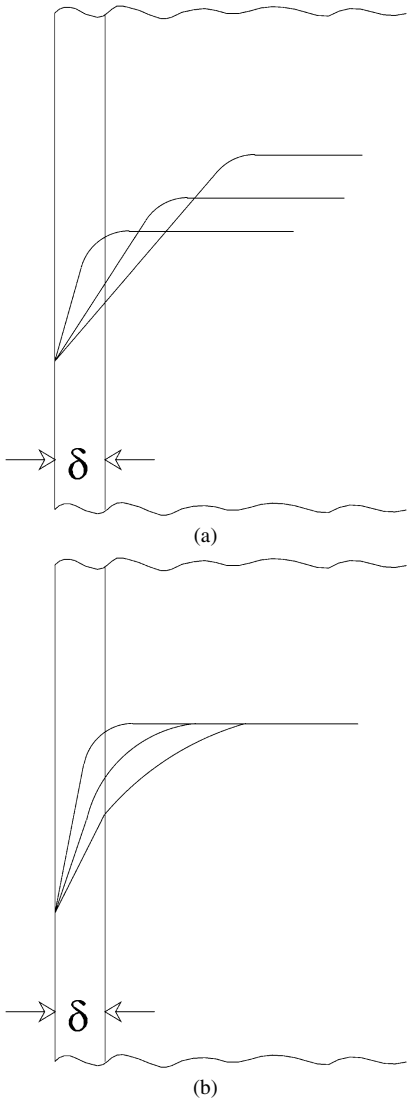

Fig. 3. Mean boundary layer thickness.

which gives

$$B_0 = \frac{2P\mathcal{L}}{\sqrt{\pi}A} \tag{47}$$

These exact limits may now be combined in a simple manner using an asymptotic correlation method.

5. Compact models

Compact models may now be developed using the asymptotic correlation method proposed by Churchill and Usagi [26]. The asymptotic limits may now be combined to develop a simple compact model for each dimensionless quantity of interest.

$$y^\star = \left[(y_0^\star)^n + (y_\infty^\star)^n\right]^{1/n} \tag{48}$$

The form for $\phi^\star$ and $\psi^\star$ is shown in Fig. 4, after Yovanovich [27]. This type of behaviour is characterized by using a negative value for the fitting parameter n, in Eq. (48).

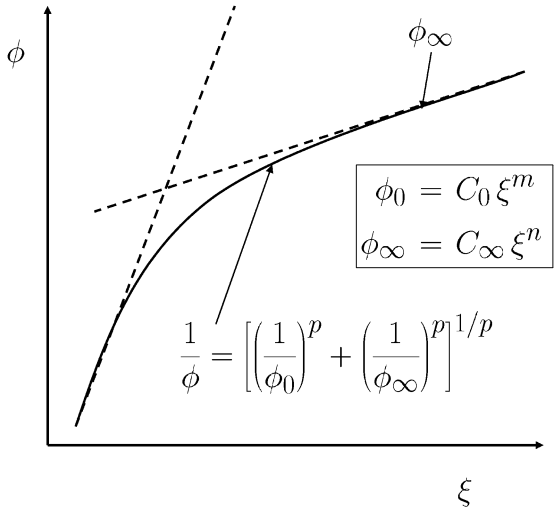

Fig. 4. Asymptotic model development.

The models of interest may now be written in the following forms:

$$\phi^\star = \left[(t^\star)^n + \left(\frac{A/P}{\mathcal{L}Po_{\mathcal{L}}}\right)^n\right]^{1/n} \tag{49}$$

and

$$\psi^\star = \left[\left(\frac{2P\mathcal{L}}{\sqrt{\pi}A}\sqrt{t^\star}\right)^p + 1\right]^{1/p} \tag{50}$$

The values of n and p may now be determined from comparisons with data obtained from the exact solutions to a number of geometries. The fitting parameters may be obtained by either applying Eqs. (49) and (50) at a single known point in the transition region or by using multiple points and minimizing the root mean square error. In the present work, the latter method is used to determine the fitting parameters.

5.1. Characteristic length scale

We shall now consider the various choices for the characteristic length scale $\mathcal{L}$. The simplest choice depending on geometry is to use the intrinsic length scale of the geometry, i.e. $\mathcal{L} = a$ for a plane wall of width $2a$ and cylinder of diameter $2a$. However, when dealing with more complex shapes, the choice for momentum transport is often the hydraulic diameter defined as $\mathcal{L} = 4A/P$. More recently, Yovanovich and Muzychka [28] and Muzychka and Yovanovich [29] have proposed using $\mathcal{L} = \sqrt{A}$ with much success in reducing Poiseuille numbers to a simple function of duct aspect ratio for momentum transport.

Examination of the proposed compact models suggests using $\mathcal{L} = 4A/P$ since it simplifies the form of the models. However, $\mathcal{L} = \sqrt{A}$ offers the advantage that the Poiseuille number is a weak function of shape and can be easily predicted for more complex shapes. The important result of Muzychka and Yovanovich [29] is that the Poiseuille numbers may be accurately predicted for the elliptic, rectangular, annular and polygonal shapes using:

$$f\,Re_{\sqrt{A}} = 2Po_{\sqrt{A}} = \frac{12}{\sqrt{\varepsilon}(1+\varepsilon)[1 - \frac{192\varepsilon}{\pi^5}\tanh(\frac{\pi}{2\varepsilon})]} \tag{51}$$

Table 2
$f\,Re$ results for elliptical and rectangular geometries [24]

$\varepsilon = b/a$	$f\,Re_{D_h}$			$f\,Re_{\sqrt{A}}$		
	Rect.	Ellip.	$\frac{f\,Re^R}{f\,Re^E}$	Rect.	Ellip.	$\frac{f\,Re^R}{f\,Re^E}$
0.01	23.67	19.73	1.200	119.56	111.35	1.074
0.05	22.48	19.60	1.147	52.77	49.69	1.062
0.10	21.17	19.31	1.096	36.82	35.01	1.052
0.20	19.07	18.60	1.025	25.59	24.65	1.038
0.30	17.51	17.90	0.978	20.78	20.21	1.028
0.40	16.37	17.29	0.947	18.12	17.75	1.021
0.50	15.55	16.82	0.924	16.49	16.26	1.014
0.60	14.98	16.48	0.909	15.47	15.32	1.010
0.70	14.61	16.24	0.900	14.84	14.74	1.007
0.80	14.38	16.10	0.893	14.47	14.40	1.005
0.90	14.26	16.02	0.890	14.28	14.23	1.004
1.00	14.23	16.00	0.889	14.23	14.18	1.004

Table 3
$f\,Re$ results for polygonal geometries [24]

N	$f\,Re_{D_h}$	$\frac{f\,Re^P}{f\,Re^C}$	$f\,Re_{\sqrt{A}}$	$\frac{f\,Re^P}{f\,Re^C}$
3	13.33	0.833	15.19	1.071
4	14.23	0.889	14.23	1.004
5	14.73	0.921	14.04	0.990
6	15.05	0.941	14.01	0.988
7	15.31	0.957	14.05	0.991
8	15.41	0.963	14.03	0.989
9	15.52	0.970	14.04	0.990
10	15.60	0.975	14.06	0.992
20	15.88	0.993	14.13	0.996
∞	16	1.000	14.18	1.000

The above expression represents a single term approximation for the rectangular duct provided $0 < \varepsilon \leqslant 1$, where $\varepsilon = b/a$ is the duct aspect ratio. Typical results are given in Tables 2 and 3 for the elliptic, rectangular, and polygonal geometries. Graphical results are provided in Figs. 5 and 6. In the case of the circular annulus $\varepsilon \approx \frac{(1-r^*)}{\pi(1+r^*)}$ where $r^* = b/a$ is the radii ratio of the annulus.

5.2. Proposed compact models

We now consider two possibilities for the characteristic length scale, $\mathcal{L}$, and develop compact models for each parameter of interest.

5.3. Hydraulic diameter, $\mathcal{L} = 4A/P$

When the hydraulic diameter is used as a characteristic length scale Eqs. (49) and (50) become:

$$\phi^\star = \left[(t^\star)^n + \left(\frac{1}{4Po_{D_h}} \right)^n \right]^{1/n} \tag{52}$$

and

$$\psi^\star = \left[\left(\frac{8}{\sqrt{\pi}} \sqrt{t^\star} \right)^p + 1 \right]^{1/p} \tag{53}$$

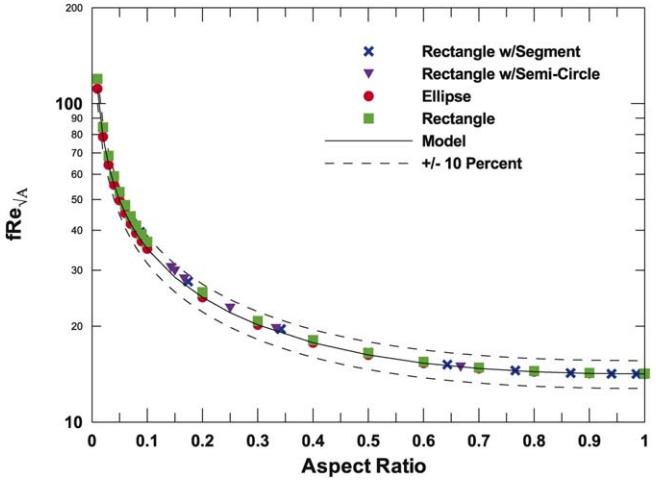

Fig. 5. $f\,Re$ for elliptic and rectangular ducts.

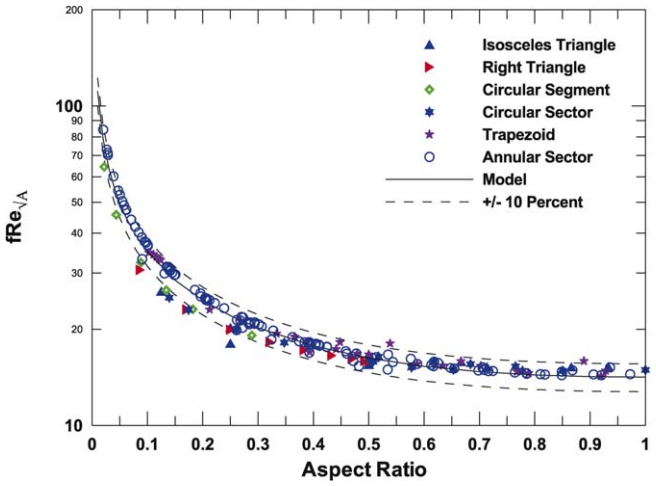

Fig. 6. $f\,Re$ for some other duct shapes.

5.4. Square root of area, $\mathcal{L} = \sqrt{A}$

When the square root of area is used as a characteristic length scale Eqs. (49) and (50) become:

$$\phi^\star = \left[(t^\star)^n + \left(\frac{\sqrt{A}/P}{Po_{\sqrt{A}}} \right)^n \right]^{1/n} \tag{54}$$

and

$$\psi^\star = \left[\left(\frac{2P/\sqrt{A}}{\sqrt{\pi}} \sqrt{t^\star} \right)^p + 1 \right]^{1/p} \tag{55}$$

The parameter $P/\sqrt{A}$ is an important geometric scaling factor. It is discussed by Yovanovich and Muzychka [28] and Muzychka and Yovanovich [29]. Further, Bejan [30] also showed its importance in a channel flows using his constructal theory of nature. The fully developed Poiseuille number has the following relationship to this geometric parameter:

$$Po_{\sqrt{A}} = Po_{D_h} \frac{P}{4\sqrt{A}} \tag{56}$$

6. Comparison with known solutions

Comparisons will now be made with four known analytical solutions: the plane channel, the circular tube, the rectangle, and the circular annulus. Each of these four geometries are closely related. The annulus contains as special limits the tube and the channel results, and the rectangle also contains the channel limit. Further, the rectangle contains the square duct which is one of the polygonal ducts which has a strong similarity to the tube and other polygonal shapes when appropriately nondimensionalized, see Table 3. In the subsequent sections, Eqs. (52) and (53) are used in presenting the model and data comparisons graphically.

6.1. Parallel plate channel

The solution for the plane channel of width $2a$ as found in [7,8,11–13,21] is:

$$\phi(y,t) = \frac{\mathcal{G}a^2}{2}\left[\left(1-\frac{y^2}{a^2}\right) - 4\sum_{n=1}^{\infty}\frac{\sin(\delta_n)}{\delta_n^3}\cos(\delta_n y/a)\exp\left(-\delta_n^2\beta t/a^2\right)\right] \quad (57)$$

where

$$\delta_n = \frac{(2n-1)\pi}{2} \quad (58)$$

It is of interest to the engineer to obtain the area mean value of ϕ as a function of time. This may be obtained by integrating the solution across the channel:

$$\overline{\phi} = \frac{1}{2a}\int_{-a}^{a}\phi(y,t)\,\mathrm{d}y \quad (59)$$

Evaluating the integral and simplifying yields

$$\overline{\phi} = \mathcal{G}a^2\left(\frac{1}{3} - 2\sum_{n=1}^{\infty}\frac{\exp(-\delta_n^2\beta t/a^2)}{\delta_n^4}\right) \quad (60)$$

Finally, the flux may be calculated from:

$$\psi = -\gamma\left.\frac{\partial\phi}{\partial y}\right|_{y=a} \quad (61)$$

or

$$\psi = \gamma\mathcal{G}a\left(1 - 2\sum_{n=1}^{\infty}\frac{\exp(-\delta_n^2\beta t/a^2)}{\delta_n^2}\right) \quad (62)$$

Eqs. (60) and (62) have been used to generate data for comparisons to the proposed models. Over the range of $0.0001 < t^\star < 10$, 50–200 terms were used in the series as required to achieve convergence. The optimal fitting parameter for $\phi^\star$ was found to be $n = -1.3$ with a root mean square error (RMS) of 6.03 percent. While for $\psi^\star$ the value was found to be $p = -6$ with a 0.262 percent RMS. Graphical results are shown in Figs. 7 and 8.

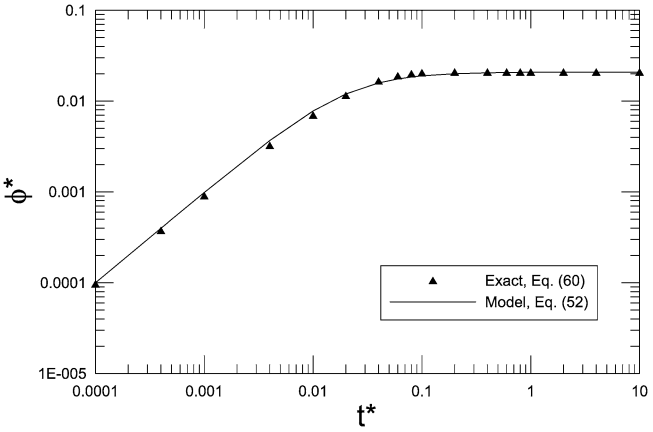

Fig. 7. $\phi^\star$ for the plane channel.

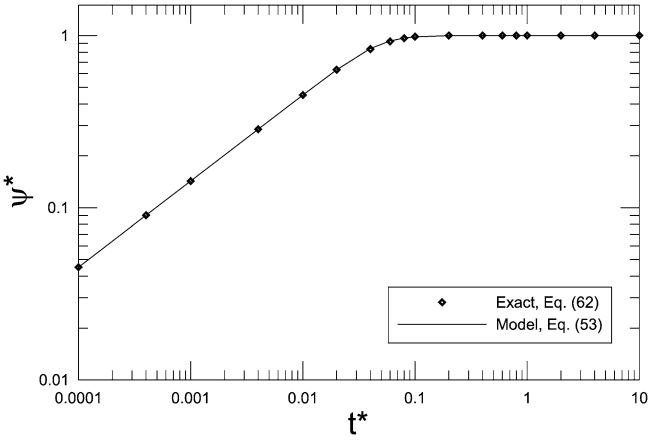

Fig. 8. $\psi^\star$ for the plane channel.

6.2. Circular tube

The solution for the circular tube of diameter $2a$ was obtained by Szymanski [6] using the separation of variables method. The solution is widely discussed in many advanced level fluid texts [1–5] and a heat conduction text [21]. The solution is:

$$\phi(r,t) = \frac{\mathcal{G}a^2}{4}\left[\left(1-\frac{r^2}{a^2}\right) - 8\sum_{n=1}^{\infty}\frac{J_o(\delta_n r/a)}{\delta_n^3 J_1(\delta_n)}\exp\left(-\delta_n^2\beta t/a^2\right)\right] \quad (63)$$

where δ_n are the positive roots of

$$J_0(\delta_n) = 0 \quad (64)$$

The mean potential may be found by integrating over the cross-sectional area

$$\overline{\phi} = \frac{2}{a^2}\int_0^a \phi(r,t) r\,\mathrm{d}r \quad (65)$$

or

$$\overline{\phi} = \mathcal{G}a^2\left(\frac{1}{8} - 4\sum_{n=1}^{\infty}\frac{\exp(-\delta_n^2\beta t/a^2)}{\delta_n^3}\right) \quad (66)$$

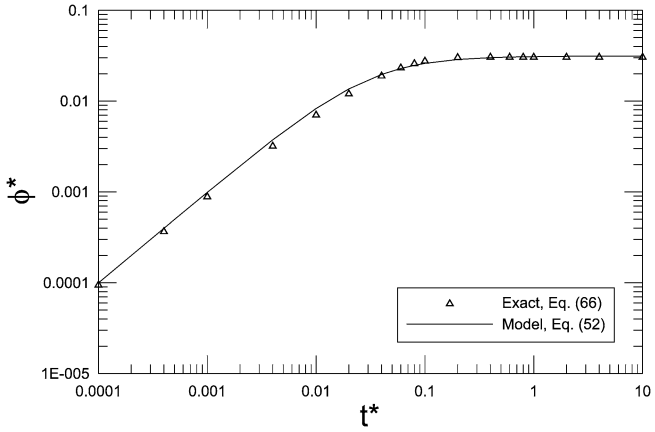

Fig. 9. $\phi^\star$ for the circular tube.

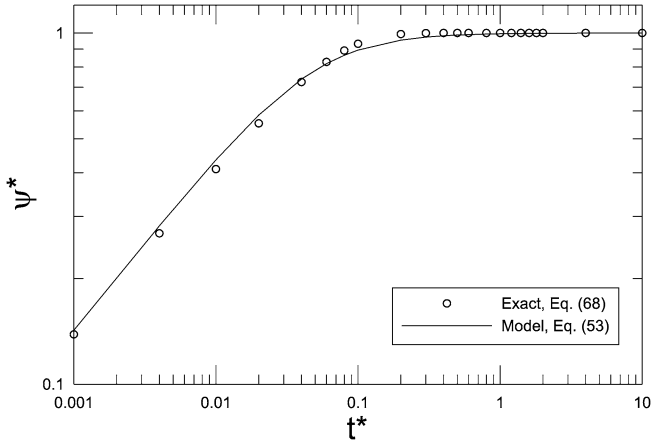

Fig. 10. $\psi^\star$ for the circular tube.

Finally, the shear stress is found from

$$\psi = -\gamma \left.\frac{\partial \phi}{\partial r}\right|_{r=a} \tag{67}$$

or

$$\psi = \gamma \mathcal{G} a \left(\frac{1}{2} - 2 \sum_{n=1}^{\infty} \frac{\exp(-\delta_n^2 \beta t / a^2)}{\delta_n^2} \right) \tag{68}$$

Eqs. (66) and (68) have been used to generate data for comparisons to the proposed models. Over the range of $0.0001 < t^\star < 10$, 50–200 terms were used in the series as required to achieve convergence. The optimal fitting parameter for $\phi^\star$ was found to be $n = -1.2$ with an RMS error of 6.94 percent. While for $\psi^\star$ the value was found to be $p = -2.8$ with an RMS error of 2.72 percent. Graphical results are shown in Figs. 9 and 10.

6.3. Rectangular channel

A search of the literature for a solution for the rectangular channel revealed a form in Erdogan [10]. The solution is quite cumbersome due to the nature of the approach taken to obtain it. The present authors have obtained the solution using the integral transform method by means of a double finite sine transform [18–20]. The solution for a rectangle having dimensions a, b with the origin placed in the lower left corner may be written in the following form:

$$\phi(x, y, t) = \frac{4}{ab} \sum_{m=1}^{\infty} \sum_{n=1}^{\infty} \frac{A_{mn}[1 - \exp(-\lambda_{mn}^2 \beta t)]}{\lambda_{mn}^2} \times \sin(m\pi x/a) \sin(n\pi y/b) \tag{69}$$

where

$$A_{mn} = \frac{\mathcal{G} ab[(-1)^m - 1][(-1)^n - 1]}{mn\pi^2} \tag{70}$$

and

$$\lambda_{mn}^2 = \frac{m^2\pi^2}{a^2} + \frac{n^2\pi^2}{b^2} \tag{71}$$

The mean potential at any time is obtained from:

$$\overline{\phi} = \frac{1}{ab} \int_0^b \int_0^a \phi(x, y, t)\, \mathrm{d}x\, \mathrm{d}y \tag{72}$$

which gives:

$$\overline{\phi} = \frac{4}{ab} \sum_{m=1}^{\infty} \sum_{n=1}^{\infty} A_{mn}\big[1 - \exp\big(-\lambda_{mn}^2 \beta t\big)\big]\big[(-1)^m - 1\big] \times \big[(-1)^n - 1\big]\big(mn\pi^2 \lambda_{mn}^2\big)^{-1} \tag{73}$$

The mean wall flux is obtained from:

$$\overline{\psi} = \frac{1}{a+b} \left[\int_0^b \gamma \left.\frac{\partial \phi}{\partial x}\right|_{x=0} \mathrm{d}y + \int_0^a \gamma \left.\frac{\partial \phi}{\partial y}\right|_{y=0} \mathrm{d}x \right] \tag{74}$$

where

$$\int_0^b \gamma \left.\frac{\partial \phi}{\partial x}\right|_{x=0} \mathrm{d}y = \frac{4\gamma}{a^2} \sum_{m=1}^{\infty} \sum_{n=1}^{\infty} \frac{A_{mn} m[1 - \exp(-\lambda_{mn}^2 \beta t)][1 - (-1)^n]}{n\lambda_{mn}^2} \tag{75}$$

and

$$\int_0^a \gamma \left.\frac{\partial \phi}{\partial y}\right|_{y=0} \mathrm{d}x = \frac{4\gamma}{b^2} \sum_{m=1}^{\infty} \sum_{n=1}^{\infty} \frac{A_{mn} n[1 - \exp(-\lambda_{mn}^2 \beta t)][1 - (-1)^m]}{m\lambda_{mn}^2} \tag{76}$$

Eqs. (73) and (74) have been used to generate data for comparisons to the proposed models. Over the range of $0.0001 < t^\star < 10$, 50–200 terms were used in the series as required to achieve convergence. Values for n and p are shown in Table 4 for various channel aspect ratios. Graphical results are shown in Figs. 11 and 12.

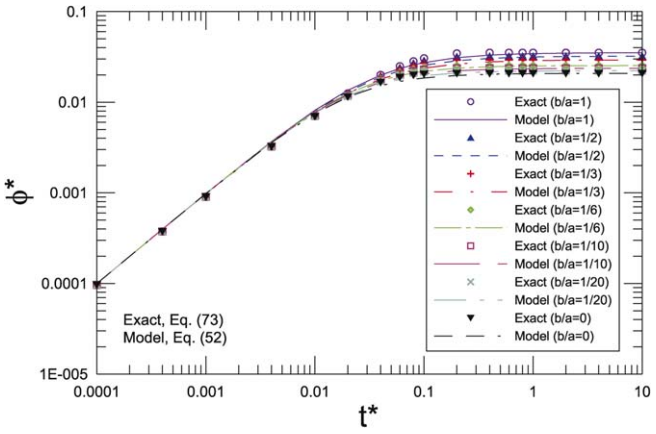

Fig. 11. $\phi^\star$ for the rectangular channel.

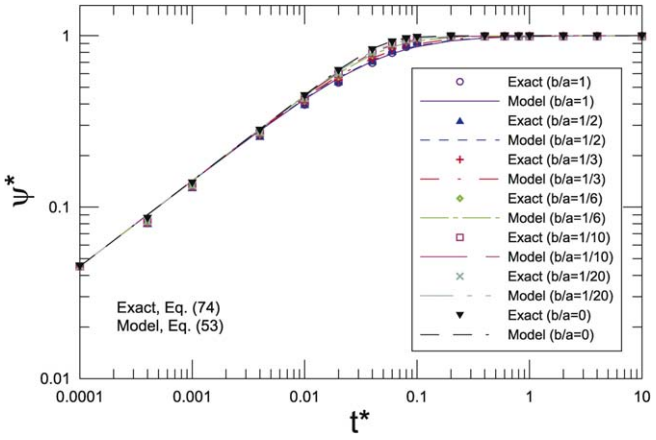

Fig. 12. $\psi^\star$ for the rectangular channel.

Table 4
Results for rectangular channel

b/a	Po_{D_h}	n	RMS	p	RMS
0	12	−1.2	6.1	−6	1.8
1/20	11.24	−1.2	6.3	−4.5	2.2
1/10	10.58	−1.2	6.1	−4	2.7
1/6	9.85	−1.2	6.4	−3.5	3.3
1/3	8.54	−1.1	6.7	−2.8	4.0
1/2	7.77	−1.1	6.9	−2.5	4.4
1	7.12	−1.1	6.9	−2.4	4.3

6.4. Circular annulus

The solution for the circular annulus with inner radius b and outer radius a, was obtained by Müller [9] using the separation of variables method. The solution which also contains Bessel functions, is much more complex than that for the tube. The final solution for the field is:

$$\phi(r,t) = \frac{\mathcal{G}a^2}{4}\left[1-\varrho^2-\frac{(1-r^{*2})\ln(1/\varrho)}{\ln(1/r^*)}\right] - \pi a^2\mathcal{G}\sum_{n=1}^{\infty}\frac{J_0(\delta_n)[J_0(\varrho\delta_n)Y_0(r^*\delta_n)-Y_0(\varrho\delta_n)J_0(r^*\delta_n)]}{\delta_n^2[J_0(\delta_n)+J_0(r^*\delta_n)]} \times \exp\left(-\delta_n^2\beta t/a^2\right) \tag{77}$$

where $r^* = b/a$, $\varrho = r/a$, and the eigenvalues, δ_n, are computed numerically from

$$J_0(\delta_n)Y_0(r^*\delta_n) - J_0(r^*\delta_n)Y_0(\delta_n) = 0 \tag{78}$$

The functions $J_0(\cdot)$ and $Y_0(\cdot)$ are Bessel functions of the first and second kind, respectively, of order zero. They are easily evaluated using the symbolic math program Maple V9 [31].

The mean potential may be found by integrating over the cross-sectional area

$$\overline{\phi} = \frac{2}{a^2-b^2}\int_b^a \phi(r,t)r\,\mathrm{d}r \tag{79}$$

which gives:

$$\overline{\phi} = \frac{\mathcal{G}a^2}{4}\left[1-r^{*2}-\frac{(1-r^{*2})}{\ln(1/r^*)}\right] - \mathcal{G}a^2\left(\frac{4}{1-r^{*2}}\right)\sum_{n=1}^{\infty}\frac{J_0(r^*\delta_n)-J_0(\delta_n)}{\delta_n^4[J_0(\delta_n)+J_0(r^*\delta_n)]} \times \exp\left(-\delta_n^2\beta t/a^2\right) \tag{80}$$

The mean wall flux is obtained from the following expression:

$$\overline{\psi} = \frac{1}{2\pi(a+b)}\left[\gamma 2\pi b\frac{\partial\phi}{\partial r}\bigg|_{r=b} - \gamma 2\pi a\frac{\partial\phi}{\partial r}\bigg|_{r=a}\right] \tag{81}$$

where

$$\gamma 2\pi b\frac{\partial\phi}{\partial r}\bigg|_{r=b} = \frac{\pi\gamma\mathcal{G}a^2}{2}\left[\left(\frac{(1-r^{*2})}{\ln(1/r^*)}-2r^{*2}\right) + 8\sum_{n=1}^{\infty}\frac{J_0(\delta_n)}{\delta_n^2[J_0(\delta_n)+J_0(r^*\delta_n)]}\exp\left(-\delta_n^2\beta t/a^2\right)\right] \tag{82}$$

and

$$-\gamma 2\pi a\frac{\partial\phi}{\partial r}\bigg|_{r=a} = \frac{\pi\gamma\mathcal{G}a^2}{2}\left[\left(2-\frac{(1-r^{*2})}{\ln(1/r^*)}\right) - 8\sum_{n=1}^{\infty}\frac{J_0(r^*\delta_n)}{\delta_n^2[J_0(\delta_n)+J_0(r^*\delta_n)]}\exp\left(-\delta_n^2\beta t/a^2\right)\right] \tag{83}$$

The above expression is easily evaluated using the symbolic math program Maple V9 [31].

Eqs. (80) and (81) have been used to generate data for comparisons to the proposed models. Over the range of $0.0001 < t^\star < 10$, 50–200 terms were used in the series as required to achieve convergence. Values for n and p are shown in Table 5 for various radii ratios. Graphical results are shown in Figs. 13 and 14.

7. Results and discussion

Examination of the data, shows that the fitting parameter n for the mean potential $\overline{\phi}$ is very nearly constant $-1.3 < n < -1.1$, with a mean value $\bar{n} = -6/5$ for all data sets. However, the fitting parameter p for the mean flux $\overline{\psi}$ varies with geometry or duct aspect ratio b/a. Values for p fall in the range

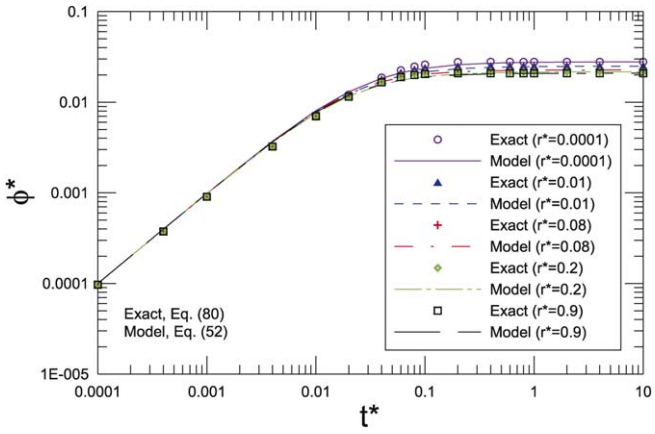

Fig. 13. $\phi^\star$ for the circular annulus.

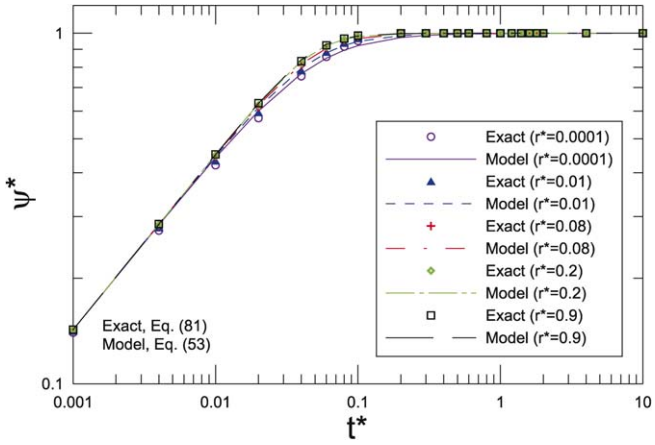

Fig. 14. $\psi^\star$ for the circular annulus.

Table 5
Results for circular annulus

b/a	Po_{D_h}	n	RMS	p	RMS
0	8	−1.2	6.9	−2.8	2.7
0.0001	8.97	−1.2	6.6	−3.3	2.1
0.01	10.01	−1.2	6.4	−4.0	1.3
0.08	11.05	−1.3	6.3	−4.8	0.61
0.20	11.54	−1.3	6.2	−5.6	0.34
0.90	11.99	−1.3	6.0	−6.0	0.24

$-6 < p < -2.4$, with the largest absolute value for the plane channel. The mean value for all data sets examined is $\overline{p} = -4$. It is proposed for simplicity, that a single value representing the mean value of n and p, be used for each model. In the case of the mean potential, this incurs a very small error due to the small range of this parameter. In the case of the mean flux, the RMS error for the channel increases to 2.21 percent from 0.26 percent, while for the tube the RMS error increases to 4.26 percent from 2.72 percent. On the whole, choosing a constant value of p provides an accuracy in the range of 2.21–7.57 percent RMS for the rectangle, and 2.21–4.26 percent RMS for the annulus.

The proposed models may also be applied to any shape for which no known solution exists. As can be seen in Eqs. (52)–(55), the only parameter which must be known apriori is the steady state Poiseuille number. Since this parameter has been determined exactly or numerically for some forty shapes [24], the models can be applied to a wide range of geometries. Further, by means of Eq. (51), Poiseuille numbers for most common shapes may be calculated within 10 percent. The effect of aspect ratio on the fitting parameter was shown to be moderate. The use of a single value introduces a small error for the sake of generality. Therefore, the proposed models may be assumed to be universal for any shape of interest.

8. Summary and conclusions

Solutions to the transient Poisson equation for the circular tube, plane channel, rectangular channel, and circular annulus were examined. These solutions are used to model either unsteady heat conduction due to a uniform heat source or unsteady viscous momentum transport due to a suddenly imposed pressure gradient. The solutions are in the form of single and double infinite series some of which require numerical solution to the eigenvalues. To facilitate computation of mean potential and mean surface flux, simple models have been proposed which allow for rapid determination of these parameters. The models are defined by Eqs. (52) and (53) or Eqs. (54) and (55) in conjunction with Eq. (51). The fitting parameters for these equations are: $\overline{n} = -6/5$ and $\overline{p} = -4$.

These models were developed by means of scale analysis and asymptotic analysis of the governing equation. The proposed models were compared with data generated from the exact solutions. Overall agreement between model and theory is quite good with an RMS error between 2–6 percent for all data examined when a single constant value of the correlation parameters was chosen. The models were also shown to be applicable to any non-circular geometry provided an exact or approximate value of the steady state Poiseuille number is known for the non-circular geometry.

Acknowledgements

The authors acknowledge the financial support of the Natural Sciences and Engineering Research Council of Canada (NSERC) through the Discovery Grants Program. The authors also thank K. Boone, Z. Duan, and M. Bahrami for assistance with the figures.

References

[1] R.B. Bird, W.E. Stewart, E.N. Lightfoot, Transport Phenomena, Wiley, New York, 1960, pp. 126–130.
[2] R.S. Brodkey, Phenomena of Fluid Motions, Dover, New York, 1967, pp. 91–95.
[3] G.K. Batchelor, Introduction to Fluid Dynamics, Cambridge University Press, Cambridge, 1970, pp. 193–195.
[4] F.M. White, Viscous Fluid Flow, McGraw-Hill, New York, 1991.
[5] D.P. Telionis, Unsteady Viscous Flows, Springer, Berlin, 1981.
[6] P. Szymanski, Quelques solutions exactes des équations de l'hydrodynamique du fluide visqueux dans le cas d'un tube cylindrique, J. Math. Pure Appl. 11 (1932) 67–107.
[7] H. Rouse (Ed.), Advanced Mechanics of Fluids, Wiley, New York, 1959, pp. 221–223.

[8] V.S. Arpaci, P. Larsen, Convection Heat Transfer, Prentice-Hall, New York, 1984, p. 73.
[9] W. Müller, Zum Problem der Anlaufstromung einer Flussigkeit im geraden Rohr mit Kreisring und Kreisquerschnitt, ZAMM 16 (1936) 227–238.
[10] M.E. Erdogan, On the flows produced by sudden application of a constant pressure gradient or by impulsive motion of a boundary, Int. J. Non-Linear Mech. 38 (2003) 781–797.
[11] H. Lamb, A paradox in fluid motion, J. London Math. Soc. 2 (1927) 109–112.
[12] T.J. Bromwich, An application of Heaviside's methods to viscous fluid motion, J. London Math. Soc. 5 (1930) 10–13.
[13] H.S. Carslaw, J.C. Jaeger, Operational Methods in Applied Mathematics, Oxford, 1948, pp. 169–170.
[14] R. Berker, Handbuch der Physik, vol. VIII, Springer, Berlin, 1963.
[15] C.Y. Wang, Exact solutions of the unsteady Navier–Stokes equations, Appl. Mech. Rev. 42 (1989) 269–282.
[16] C.Y. Wang, Exact solutions of the steady state Navier–Stokes equations, Annu. Rev. Fluid Mech. 23 (1991) 159–177.
[17] M.E. Erdogan, On the unsteady unidirectional flows generated by impulsive motion of a boundary or sudden application of pressure gradient, Int. J. Non-Linear Mech. 37 (2002) 1091–1106.
[18] I.N. Sneddon, Fourier Transforms, Dover, New York, 1951.
[19] I.N. Sneddon, The Uses of Integral Transforms, McGraw-Hill, New York, 1972.
[20] R.V. Churchill, Operational Mathematics, McGraw-Hill, New York, 1972.
[21] H.S. Carslaw, J.C. Jaeger, Conduction of Heat in Solids, Oxford, 1959, pp. 130–131, 204–205.
[22] G. Thews, Uber die Mathematiische Behandlung Physiologischer Diffusionsprozesse in Zylinderformigen Objekten, Acta Biotheoretica A 10 (1953) 105–138.
[23] A. Bejan, Convection Heat Transfer, Wiley, New York, 1995.
[24] R.K. Shah, A.L. London, Laminar Flow Forced Convection in Ducts, Academic Press, New York, 1978.
[25] S.W. Yuan, Foundations of Fluid Mechanics, Prentice-Hall, Englewood Cliffs, NY, 1967, pp. 291–293.
[26] S.W. Churchill, R. Usagi, A general expression for the correlation of rates of transfer and other phenomena, Amer. Instit. Chem. Eng. 18 (1972) 1121–1128.
[27] M.M. Yovanovich, Asymptotes and asymptotic analysis for development of compact models for microelectronics cooling, Keynote Address, Semitherm 2003, San Jose, CA, March 2003.
[28] M.M. Yovanovich, Y.S. Muzychka, Solutions of Poisson equation in singly and doubly connected prismatic bars, AIAA Paper 97-3880, 1997 National Heat Transfer Conference, Baltimore, MD, 1997.
[29] Y.S. Muzychka, M.M. Yovanovich, Laminar flow friction and heat transfer in non-circular ducts—Part I. Hydrodynamic problem, in: G.P. Celata, B. Thonon, A. Bontemps, S. Kandlikar (Eds.), Compact Heat Exchangers—A Festschrift on the 60th Birthday of Ramesh K. Shah, Edizioni ETS, 2002, pp. 123–130.
[30] A. Bejan, Shape and Structure: From Engineering to Nature, Cambridge, 2000.
[31] Maple V9, Waterloo Maple Software, 2003.